Avobenzone, Guaiazulene and Tioxolone identified as potent autophagy inducers in a high-throughput image based screen for autophagy flux

Surendra Kumar Prajapat, Chandru Subramani [1], Puja Sharma, Sudhanshu Vrati & Manjula Kalia*

Regional Centre for Biotechnology, NCR Biotech Science Cluster, Faridabad, 121001, Haryana, India

*Correspondence: Manjula Kalia, manjula@rcb.res.in

[1]Present address: Department of Pathology, University of Texas medical branch, Galveston, Texas 77550

Keywords: FDA drugs**;** GFP-LC3-RFP; High content screening; Microsource spectrum library; mTOR

Abstract

Autophagy is a conserved intracellular degradation pathway that is essential for maintaining cellular homeostasis. Given its critical role in several disease conditions, recent studies are focussed on identifying drugs/small molecules with autophagy modulating capacity for potential clinical applications. Here, we describe the development and characterisation of a quantitative image-based high content screening platform for autophagy flux measurements using the human melanoma A375 cell line that stably expresses the GFP-LC3-RFP probe. The GFP-LC3 is incorporated into autophagosomes, while RFP serves an internal control. The GFP/RFP fluorescence intensity ratio gives an accurate indication of autophagy induction (low ratio) vs blockage of autophagy flux (high ratio), and was validated with the autophagy inducer Torin1 and inhibitor Bafilomycin A_1. This assay was used to screen the Spectrum collection library comprising of 2560 compounds, to identify autophagy modulators. In addition to known autophagy effectors, several novel autophagy inducers and inhibitors were identified in our study. Further three FDA approved drugs that are widely used in skin-care products: Avobenzone, Guaiazulene and Tioxolone, were validated as potent autophagy inducers that function in an mTOR independent manner.

Abbreviations: Baf, Bafilomycin A_1; LC3, Microtubule-associated protein light chain 3; mTOR, mechanistic target of rapamycin

Introduction

Macroautophagy (hereafter, autophagy) is an intracellular degradative pathway, conserved from yeast to human. It occurs at a basal level to maintain cellular homeostasis, and is upregulated during starvation and disease conditions [1]. Recent studies have shown that pharmacological modulation of autophagy holds tremendous therapeutic potential for disease conditions such as neurodegeneration and cancer [2], and hence identification of autophagy modulating drugs/compounds is an active area of research [3].

The measurement of autophagy is done by monitoring the lipidated levels of microtubule-associated protein light chain 3 (LC3) protein that specifically incorporates into autophagosomes. Other techniques involve direct visualization of autophagosomes through fluorescence or electron microscopy. The degradative capacity of the pathway or autophagy flux is analysed by using specific inhibitors of autophagosome-lysosome fusion either through western blotting for LC3-II levels or by using ratiometric fluorescence based assays [4-6]. These have been further developed for high throughput platforms and can enable testing the autophagy capacity of several thousand compounds. A series of image based high throughput screening studies using probes such as mRFP-GFP-LC3, GPF-LC3-RFP-LC3ΔG, GFP-LC3-RFP etc. have identified autophagy inducers with broad translation potential [6-10].

Here we have developed an image-based high content quantitative assay using the human melanoma A375 cell line stably expressing the fluorescent probe GFP-LC3-RFP [6]. In a primary screening of the Microsource spectrum library, several autophagy flux inducers and inhibitors were identified by low and high GFP/RFP signal ratios respectively. Three drugs widely used in skin-care products Avobenzone, Guaiazulene and Tioxolone, were further validated for their autophagy inducing properties.

Results

Generation and validation of A375 cell line stably expressing autophagy flux probe

Studies have established that the GFP-LC3-RFP probe is a powerful tool for measurements of autophagy flux [5,6,11]. This protein is cleaved by the cellular cysteine protease ATG4, into two equimolar fragments of GFP-LC3 and RFP. The GFP-LC3 is lipidated with phosphatidylethanolamine (PE) at the terminal glycine residue, resulting in its incorporation into autophagosomes. Depending on the status of autophagy in the cell, the levels of GFP-LC3 change, while the RFP serves as an internal control (Fig 1A). The ratiometric measurements of GFP/RFP relative to a basal/untreated condition are an accurate reflection of autophagy induction or inhibition in the cell (Fig 1A) [6,12].

We generated a stable human melanoma A375 cell line expressing this autophagy flux probe (Fig 1B). Positive clones were validated, and one clone for chosen for further studies. The GFP-LC3 expression was detected using both GFP and LC3 antibodies (Fig 1B). Roughly equal levels of RFP were also seen (Fig 1B). Fluorescence images showed that the clone expressed GFP-LC3 and showed punctate distribution in the cell corresponding to autophagosomes, while diffuse RFP staining was observed throughout the cytosol (Fig 1C, upper panel). Non-toxic concentrations of Torin1 (autophagy inducer), and Bafilomycin A_1 (Baf) (autophagosome-lysosome fusion inhibitor), were determined (Fig S1A-B). Treatment of these cells with Torin1, resulted in a clear reduction in GFP-fluorescence in these cells, while treatment with Baf showed enhanced GFP intensity (Fig 1C). GFP/RFP ratios in the Torin1 and Baf treated cells were normalized to DMSO treated cells. Torin1 treatment showed a clear reduction of GFP/RFP ratio indicative of high autophagy flux, while Baf showed an enhanced ratio indicative of low autophagy flux (Fig 1D). These data established the validity of this cell line for autophagy flux measurements.

Establishment of a high content screening platform

This cell line was next tested in a high throughput 96 well plate platform. Cells were treated with DMSO (control) or Torin1/ Baf, and images were acquired. As seen earlier through confocal microscopy, Torin1 and Baf treatment resulted in reduced and enhanced GFP/RFP ratios respectively (Fig 2A, S1C-D). Based on values obtained with Torin1 and Baf, we established a cut off limit of <0.8 for autophagy inducers and >1.2 for autophagy inhibitors (Fig 2B). Using this technique, we screened the Spectrum library of 2560 compounds at 10 µM concentration. Control, Torin1, Baf, and drug treatments were given for 12 h. The cytotoxicity of the drug treatment was established through DAPI staining compared to untreated controls as described in the methods section (Data Sheet S1). Based on the GFP/RFP ratios, we identified 104 drugs that changed the cellular autophagy levels (Fig 2C-D, Fig S2, File S1). The autophagy inducers (Fig 2C) and inhibitors (Fig 2D) were classified based on their reported biological activities in literature. Of these 53 drugs have been previously established as autophagy inducers in literature [6,7,9]. We further identified 31 novel autophagy inducers and 19 novel autophagy inhibitors (File S1).

Avobenzone, Guaiazulene and Tioxolone identified as potent autophagy inducers

Of the shortlisted drugs, we focused our attention on three FDA-approved drugs that are widely used in skin-care products: Avobenzone, Guaiazulene and Tioxolone. All the drugs were retested for toxicity (Fig 3A), and showed GFP/RFP ratios comparable to Torin1 (Fig 3B, C), identifying them as potent autophagy inducers. We also checked these drugs with the ptfLC3 reporter [5], and observed an increase in the number of autophagosomes ($mRFP^{+}/GFP^{+}$) and autolysosomes ($mRFP^{+}/GFP^{-}$) on drug treatment, that was comparable to Torin1 (Fig S3). Lysosome acidification was checked with the LysoSensor Yellow- Blue assay [13], and was found to be similar to Torin1 treatment (Fig S4). We further validated autophagy induction through western blotting for LC3. All the drugs showed enhanced LC3-II levels (Fig 4A-C). By using Baf we confirmed that LC3-II accumulation caused by these

drugs was due to autophagy induction and not due to blockage of autophagosome-lysosome fusion (Fig 4A-C). Levels of p62 clearance were also assessed through western blotting and these showed a reduction compared to DMSO treatment (Fig 4D-E), but did not have any effect on p62 mRNA levels (Fig 4F). We also tested if these drugs acted in an mTOR dependent manner by checking phosphorylation levels of S6 kinase (S6K) and eukaryotic translation initiation factor 4E-binding protein 1 (4E-BP1). While Torin1 resulted in efficient dephosphorylation of S6K and 4E-BP1, these drugs had no effect on phosphorylation of S6K and 4E-BP1 (Fig 4G-H), suggesting that their mode of action is mTOR independent.

Discussion

Autophagy research has rapidly evolved and interest has heightened on examining the potential of novel/existing drugs to modulate autophagy [14]. Autophagy modulation is likely to have therapeutic benefits in several disease conditions [15]. Conversely, several FDA-approved drugs could be autophagy modulators but have not been studied from this perspective.

In our current study, we developed a reporter cell line for high throughput measurements of autophagy flux, and identified several known and novel autophagy modulators in the Spectrum collection library of 2560 compounds. Our primary screening and validation showed that three FDA-approved drugs that are widely used in skin-care preparations: avobenzone, guaiazulene, and tioxolone can efficiently induce autophagy flux in an mTOR independent manner.

Avobenzone (butyl methoxydibenzoylmethane; parsol 1789) is an ultraviolet A absorber widely used in sunscreens [16-22]. Studies have shown that avobenzone can efficiently penetrate the stratum corneum and viable epidermis [23]. It has been shown to protect against UVA-induced melanogenesis through indirect regulatory effect on the Nrf2-ARE pathway [24]. It has also been shown to inhibit the proliferation of human trophoblasts, enhance Akt and ERK1/2 activity and induce mitochondrial membrane depolarization [25]. In normal human epidermal keratinocytes, it can downmodulate lipid metabolism, and Peroxisome proliferator-activated receptor-gamma signaling [26], and can induce keratinocyte derived Vascular endothelial growth factor production [27]. Its autophagy inducing properties have not been described till date, however based on the above-mentioned studies, it is likely that autophagy will play an important role in the mode of action of avobenzone.

Guaiazulene (1,4-dimethyl-7-isopropylazulene), is a natural azulenic compound widely used in cosmetic and health-care products and in pharmaceutical preparations such as creams and

144 toothpastes [28,29]. Its early use was as an ophtlamic drug, and later it became a popular skin
145 conditioning agent. The drug was also shown to be promising for the treatment of gastritis
146 and peptic ulcers [30]. Studies have shown that it can act in a synergic manner with
147 diclofenac and can have therapeutic advantages for the clinical treatment of inflammatory
148 pain [31]. It has also been shown to have anti-cancer properties [32]. A recent study showed
149 that guaiazulene inhibited Akt/mTOR signalling and induced autophagosome formation [33].
150 However, this study used a very high concentration of guaiazulene (100/150 μM), which
151 might account for the observed mTOR inhibition.
152 Tioxolone (6-Hydroxy-2H-1,3-benzoxathiol-2-one) is used for cosmetics products such as
153 hair shampoos, skin cleansers and acne treatment products [34]. It has anti-fungal, anti-
154 bacterial, anti-inflammatory and anti-tumorigenic effects, and has been shown to be an
155 inhibitor of human carbonic anhydrase II [35,36]. Tincture of thioxolone plus benzoxonium
156 chloride was shown to be useful for the treatment of cutaneous leishmaniasis [37].
157 In summary, our high throughput screening approach has identified several novel autophagy
158 inducers and inhibitors. We also validate that three widely used drugs in skin-care products
159 are potent autophagy inducers. Further studies will highlight if the autophagy inducing
160 properties of these drugs govern their mode of action.

Materials and Methods

Cell lines

A375 and HEK293T cells were obtained from the Cell Repository at the National Centre for Cell Sciences, Pune, India. Cells were grown in Dulbecco's modified Eagle's medium (DMEM) (HiMedia, AL007A) supplemented with 10% fetal bovine serum (FBS) (HiMedia, RM10432), 100 µg/ml penicillin-streptomycin, 2 mM L-glutamine and 1x MEM Non-Essential Amino Acids Solution (HiMedia, ACL006).

Reagents, antibodies and plasmids

The following reagents were used in the study: Torin1 (Tocris Bioscience, 4247), Bafilomycin (Baf)-A1 (Sigma-Aldrich, B1793-10UG), PMSF (Sigma-Aldrich, P7626-100G), Protease inhibitor cocktail (Sigma-Aldrich, 11697498001), LysoSensor Yellow/Blue DND-160 (Thermo Fisher Scientific, L7545). The Spectrum collection library (MicroSource Discovery Systems, Inc., SP170615) comprising of 2560 compounds including bioactive molecules, natural products, and FDA-approved compounds was used for image based high content screening. The following antibodies were used in the study: GAPDH (14C10); Phospho-4E-BP (Thr37/46) (2855S); 4E-BP (9644S); Phospho-p70 S6 Kinase (Thr389) (97596S) and p70 S6 Kinase (2708S) from Cell Signalling Technology, LC3 (ab51520); RFP (ab62341), GFP (ab32146) and SQSTM1/p62 (ab56416) from Abcam, HRP-conjugated secondary antibodies from Jackson ImmunoResearch Laboratories. The following plasmids were obtained from Addgene: gag/pol (14887, Tannishtha Reya) [38], pCI-VSVG (1733, Garry Nolan) [39], pMRX-IP-GFP-LC3-RFP (84573, Noboru Mizushima) [6], and ptfLC3 (21074, Tamotsu Yoshimori) [10]. The following primers (5□-3□) were used in the study GAPDH: F-TGCACCACCAACTGCTTAGC, R-GGCATGGACTGTGGTCATGAG; P62/SQSTM1: F-AGGCGCACTACCGCGAT, R-CGTCACTGGAAAAGGCAACC.

Stable cell line generation

HEK293T cells were co-transfected with gag/pol, pCI-VSVG and pMRX-IP-GFP-LC3-RFP plasmids using Lipofectamine 2000 and incubated at 37°C for 24 h. The supernatant was harvested for retrovirus, and was used to transduce A375 cells. Puromycin selection (2 µg/ml) was given after 48 h. After one week of selection, cells were trypsinized and 10,000 cells were serially diluted to achieve single cell seeding per well of a 96 well-plate. Isolated colonies were visible by 14 days, and were tested for the expression of GFP, RFP and autophagy flux using Torin1 and Baf treatments. One clone was chosen for further studies.

Drug treatment & confocal imaging

Stable GFP-LC3-RFP A375 cells or A375 cells transiently transfected with ptfLC3, were treated with Torin1 (1 µM/ 6h; 100 nM/ 12h) or Baf (100 nM/ 6h; 20 nM/ 12h) or DMSO/Avobenzone/ Guaiazulene Tioxolone (10 µM) for 12 h. For confocal microscopy all cells were grown on glass coverslips. GFP/RFP intensity ratio per cell was calculated and normalized to DMSO control treated cells. For ptfLC3 experiments, autophagosomes (RFP^+/GFP^+ structures) and autolysosomes (RFP^+/GFP^- structures) per cell were counted using Spot to Spot colocalization analysis in Imaris 8.

High content imaging and analysis

For image based high content screening 15,000 cells/well were seeded in Corning 96 well black polystyrene microplates (Corning, CLS3603). Torin1 (100 nM), Baf (20 nM), and drug (10 µM) treatment was given for 12 h. All drugs were tested in biological duplicates or triplicates. Cells were fixed and stained with DAPI. Images were acquired on ImageXpress Micro Confocal High-Content Imaging System (Molecular Devices, USA) using FITC, Texas red, and DAPI channels with a 10 X objective lens. A total of 16 fields per well were acquired and this covered the entire well area. Analysis was performed using the multi-wavelength cell scoring module of the MetaXpress Software. To calculate drug cytotoxicity, total nuclei were counted using DAPI in drug and DMSO treated wells. Any drug showing

more than 20% reduction in total nuclei was considered as toxic and excluded from further analysis. Only triple positive cells (DAPI, GFP, RFP) were used for quantitation. The integral intensity of GFP and RFP per well was calculated and used to estimate the GFP/RFP ratio. The values obtained for DMSO treatment were used for normalization. The GFP/RFP ratio in Torin1 treatment gave a mean value of 0.68, while BafA1 treatment gave a mean value of 1.2. Any drug showing a GFP/RFP ratio <0.8 was considered as an autophagy inducer, and GFP/RFP ratio >1.2 was marked as autophagy flux inhibitor.

Western blotting

After drug treatment A375 cells were washed with PBS and lysed using cell lysis buffer [150 mM NaCl, 1% Triton X-100, 50 mM Tris-HCl (pH 7.5), 200 µM PMSF and protease inhibitor cocktail]. Protein quantification was done using BCA assay (G-Bioscience, 786-570) kit. Cell lysates were separated on polyacrylamide gels and transferred to a PVDF membrane for immunoblotting using specific primary and secondary antibodies. Western blot images were processed using ImageJ (NIH, USA) software for quantitation of band intensities. Data are represented as mean ± SD from three independent experiments.

LysoSensor Yellow- Blue assay

The LysoSensor Yellow-Blue assay was performed as described in [13]. A375 cells were were grown on glass coverslips, and were treated with DMSO (control), Torin1 (1 µM) or Baf (100 nM) or Avobenzone/ Guaiazulene Tioxolone, followed by incubation with 10 µM LysoSensor for 5 min. Cells were then washed with ice-cold PBS three times and fixed using 4% PFA. Cells were imaged on LSM 880, Carl Zeiss, with excitation wavelength range 371-405 nm and emission wavelength range 420-650 nm. The LysoSensor dye has dual-emission peaks of 440 nm (blue in less acidic organelles) and 540 nm (yellow in more acidic organelles). Yellow fluorescence per cell was quantified and normalized to DMSO treated control.

Cell viability assay

A375 cells were seeded at a density of 15000 cells/well in 96-well plates. After 24 h, cells were treated with indicated concentrations of Torin1/ Baf/ Avobenzone/ Guaiazulene Tioxolone for 6 or 12 h. The cytotoxicity assay was performed using CellTiter-Glo kit (Promega, G7572). Percentage of cell viability was measured relative to DMSO treated cells.

Statistical analysis

Statistical analysis of the data was performed using one-way ANOVA and differences were considered significant at values of $*P < 0.05$, $**P < 0.01$, $***P < 0.001$, $**** P < 0.0001$

Conflict of interest

The authors have no conflict of interest to declare

Acknowledgements

High content screening was performed at the Advanced Technology Platform Centre (ATPC) at RCB. We are thankful to Dr. Nirpendra Singh, Ashish Pandey and Rajan for technical support. Simran Chhabra and all other Virology lab members are acknowledged for their support and suggestions.

Funding

This work was supported by a grant from DBT BT/PR27875/Med/29/1302/2018, and from DBT intra-mural funds to RCB. SKP is supported by a DBT-SRF fellowship. PS is supported by UGC-SRF fellowship.

References:

1. Mizushima N, Levine B, Cuervo AM, et al. Autophagy fights disease through cellular self-digestion. Nature. 2008 Feb 28;451(7182):1069-75.

2. Vakifahmetoglu-Norberg H, Xia HG, Yuan J. Pharmacologic agents targeting autophagy. The Journal of clinical investigation. 2015 Jan;125(1):5-13.

3. Choi AM, Ryter SW, Levine B. Autophagy in human health and disease. The New England journal of medicine. 2013 Feb 14;368(7):651-62.

4. Klionsky DJ, Abdel-Aziz AK, Abdelfatah S, et al. Guidelines for the use and interpretation of assays for monitoring autophagy (4th edition)(1). Autophagy. 2021 Jan;17(1):1-382.

5. Mizushima N, Yoshimori T, Levine B. Methods in mammalian autophagy research. Cell. 2010 Feb 5;140(3):313-26.

6. Kaizuka T, Morishita H, Hama Y, et al. An Autophagic Flux Probe that Releases an Internal Control. Molecular cell. 2016 Nov 17;64(4):835-849.

7. Chauhan S, Ahmed Z, Bradfute SB, et al. Pharmaceutical screen identifies novel target processes for activation of autophagy with a broad translational potential. Nature communications. 2015 Oct 27;6:8620.

8. Li Y, McGreal S, Zhao J, et al. A cell-based quantitative high-throughput image screening identified novel autophagy modulators. Pharmacological research. 2016 Aug;110:35-49.

9. Zhang L, Yu J, Pan H, et al. Small molecule regulators of autophagy identified by an image-based high-throughput screen. Proceedings of the National Academy of Sciences of the United States of America. 2007 Nov 27;104(48):19023-8.

10. Kimura S, Noda T, Yoshimori T. Dissection of the autophagosome maturation process by a novel reporter protein, tandem fluorescent-tagged LC3. Autophagy. 2007 Sep-Oct;3(5):452-60.

11. Geng J, Klionsky DJ. Direct quantification of autophagic flux by a single molecule-based probe. Autophagy. 2017 Apr 3;13(4):639-641.

12. Huang L, Fu Q, Dai J-M, et al. High-content screening of diterpenoids from Isodon species as autophagy modulators and the functional study of their antiviral activities. Cell Biology and Toxicology. 2021 2021/01/23.

13. Albrecht LV, Tejeda-Muñoz N, De Robertis EM. Protocol for Probing Regulated Lysosomal Activity and Function in Living Cells. STAR protocols. 2020 Dec 18;1(3):100132.

14. Kataura T, Tashiro E, Nishikawa S, et al. A chemical genomics-aggrephagy integrated method studying functional analysis of autophagy inducers. Autophagy. 2021 Aug;17(8):1856-1872.

15. Yao RQ, Ren C, Xia ZF, et al. Organelle-specific autophagy in inflammatory diseases: a potential therapeutic target underlying the quality control of multiple organelles. Autophagy. 2021 Feb;17(2):385-401.

16. Callen JP, Roth DE, McGrath C, et al. Safety and efficacy of a broad-spectrum sunscreen in patients with discoid or subacute cutaneous lupus erythematosus. Cutis. 1991 Feb;47(2):130-2, 135-6.

17. Hanson KM, Clegg RM. Bioconvertible vitamin antioxidants improve sunscreen photoprotection against UV-induced reactive oxygen species. Journal of cosmetic science. 2003 Nov-Dec;54(6):589-98.

18. Chatelain E, Gabard B. Photostabilization of butyl methoxydibenzoylmethane (Avobenzone) and ethylhexyl methoxycinnamate by bis-ethylhexyloxyphenol

methoxyphenyl triazine (Tinosorb S), a new UV broadband filter. Photochemistry and photobiology. 2001 Sep;74(3):401-6.

19. Gonzaga ER. Role of UV light in photodamage, skin aging, and skin cancer: importance of photoprotection. American journal of clinical dermatology. 2009;10 Suppl 1:19-24.

20. Wang SQ, Stanfield JW, Osterwalder U. In vitro assessments of UVA protection by popular sunscreens available in the United States. Journal of the American Academy of Dermatology. 2008 Dec;59(6):934-42.

21. Beasley DG, Meyer TA. Characterization of the UVA protection provided by avobenzone, zinc oxide, and titanium dioxide in broad-spectrum sunscreen products. American journal of clinical dermatology. 2010 Dec 1;11(6):413-21.

22. Kockler J, Robertson S, Oelgemöller M, et al. Butyl methoxy dibenzoylmethane. Profiles of drug substances, excipients, and related methodology. 2013;38:87-111.

23. Hayden CG, Cross SE, Anderson C, et al. Sunscreen penetration of human skin and related keratinocyte toxicity after topical application. Skin pharmacology and physiology. 2005 Jul-Aug;18(4):170-4.

24. Chaiprasongsuk A, Onkoksoong T, Pluemsamran T, et al. Photoprotection by dietary phenolics against melanogenesis induced by UVA through Nrf2-dependent antioxidant responses. Redox biology. 2016 Aug;8:79-90.

25. Yang C, Lim W, Bazer FW, et al. Avobenzone suppresses proliferative activity of human trophoblast cells and induces apoptosis mediated by mitochondrial disruption. Reproductive toxicology (Elmsford, NY). 2018 Oct;81:50-57.

26. Ahn S, An S, Lee M, et al. A long-wave UVA filter avobenzone induces obesogenic phenotypes in normal human epidermal keratinocytes and mesenchymal stem cells. Archives of toxicology. 2019 Jul;93(7):1903-1915.

27. Bae ON, Ahn S, Jin SH, et al. Chemical allergens stimulate human epidermal keratinocytes to produce lymphangiogenic vascular endothelial growth factor. Toxicology and applied pharmacology. 2015 Mar 1;283(2):147-55.

28. Fiori J, Gotti R, Albini A, et al. Study on the photostability of guaiazulene by high-performance liquid chromatography/mass spectrometry and gas chromatography/mass spectrometry. Rapid communications in mass spectrometry : RCM. 2008 Sep;22(17):2698-706.

29. Fiori J, Gotti R, Valgimigli L, et al. Guaiazulene in health care products: determination by GC-MS and HPLC-DAD and photostability test. J Pharm Biomed Anal. 2008 Aug 5;47(4-5):710-5.

30. Okabe S, Takeuchi K, Mori Y, et al. [Effects of KT1-32 on acute gastric lesions and duodenal ulcers induced in rats]. Nihon Yakurigaku Zasshi. 1986 Dec;88(6):467-76.

31. Ortiz MI, Fernandez-Martinez E, Soria-Jasso LE, et al. Isolation, identification and molecular docking as cyclooxygenase (COX) inhibitors of the main constituents of Matricaria chamomilla L. extract and its synergistic interaction with diclofenac on nociception and gastric damage in rats. Biomed Pharmacother. 2016 Mar;78:248-256.

32. Teratani M, Nakamura S, Sakagami H, et al. Antitumor Effects and Tumor-specificity of Guaiazulene-3-Carboxylate Derivatives Against Oral Squamous Cell Carcinoma In Vitro. Anticancer Res. 2020 Sep;40(9):4885-4894.

33. Ye Q, Zhou L, Jin P, et al. Guaiazulene Triggers ROS-Induced Apoptosis and Protective Autophagy in Non-small Cell Lung Cancer. Front Pharmacol. 2021;12:621181.

34. Tao Y, Wang Q, Sun K, et al. The molecular structure, spectroscopic features and electronic properties of tioxolone under the external electric field. Spectrochimica acta Part A, Molecular and biomolecular spectroscopy. 2020 Apr 15;231:118108.

35. Iyer R, Barrese AA, 3rd, Parakh S, et al. Inhibition profiling of human carbonic anhydrase II by high-throughput screening of structurally diverse, biologically active compounds. Journal of biomolecular screening. 2006 Oct;11(7):782-91.

36. Barrese AA, 3rd, Genis C, Fisher SZ, et al. Inhibition of carbonic anhydrase II by thioxolone: a mechanistic and structural study. Biochemistry. 2008 Mar 11;47(10):3174-84.

37. Daie Parizi MH, Karvar M, Sharifi I, et al. The topical treatment of anthroponotic cutaneous leishmaniasis with the tincture of thioxolone plus benzoxonium chloride (Thio-Ben) along with cryotherapy: a single-blind randomized clinical trial. Dermatol Ther. 2015 May-Jun;28(3):140-6.

38. Reya T, Duncan AW, Ailles L, et al. A role for Wnt signalling in self-renewal of haematopoietic stem cells. Nature. 2003 May 22;423(6938):409-14.

39. Zhang P, Rausch C, Hastert FD, et al. Methyl-CpG binding domain protein 1 regulates localization and activity of Tet1 in a CXXC3 domain-dependent manner. Nucleic acids research. 2017 Jul 7;45(12):7118-7136.

Figure Legends

Figure 1. Development of GFP-LC3-RFP cell-line for autophagy flux assays. (A) Schematic representation of the autophagy flux measurement assay using the GFP-LC3-RFP fluorescent probe. (B) The stable A375 (GFP-LC3-RFP) clone was analysed by western blotting using GFP, RFP and LC3 antibodies. Cleavage of the GFP-LC3 from the RFP fragment is observed. Endogenous LC3 bands can be seen in a higher exposure (H.E) blot on the extreme right (C) A375 (GFP-LC3-RFP) cells were treated with DMSO or autophagy inducer Torin1 (1 µM) or inhibitor Baf (100 nM) for 6 h. Cells were imaged on a confocal microscope. Scale bar 200 µm. (D) GFP/RFP intensity ratios were measured from 20-30 cells from two independent coverslips and normalized to DMSO control. One-way ANOVA was used to determine statistical significance, ***$P < 0.001$, **** $P < 0.0001$

Figure 2. High throughput imaging screen of Microsource spectrum library. (A) The Microsource spectrum library consisting of 2560 drugs were screened for the identification of autophagy flux modulators. A375 (GFP-LC3-RFP) cells were treated with DMSO/ Torin1 (100 nM)/ Baf (20 nM)/ drugs (10 µM) for 12 h in biological duplicates or triplicates. Images were acquired using the Image Xpress high content imaging system, and representative images are shown. Scale bar 100 µm. (B) GFP/RFP ratios were measured and normalized to DMSO control. Values show relative GFP/RFP ratios from 3 independent experiments. (C-D) Venn diagram showing the categorical classification of different molecules identified as autophagy inducers (ratio <0.8) or inhibitors (ratio >1.2). One-way ANOVA was used to determine statistical significance, **** $P < 0.0001$

Figure 3. Avobenzone, Guaiazulene and Tioxolone are autophagy inducers. (A) Viability measurements of A375 cells treated with Avobenzone/ Guaiazulene/ Tioxolone (10 µM) for 12 h. (B-C) A375 (GFP-LC3-RFP) cells were treated with DMSO, drugs (Torin1/ Baf) or Avobenzone/ Guaiazulene/ Tioxolone (n=3), and images were acquired using the Image

Xpress high content imaging system. The relative ratiometric quantitation of GFP/RFP normalized to DMSO control is plotted in (C). One-way ANOVA was used to determine statistical significance, ***$P < 0.001$, **** $P < 0.0001$.

Figure 4. Characterization of Avobenzone, Guaiazulene and Tioxolone as autophagy inducers. (A-B) A375 cells were treated with the indicated drugs (10 μM) for 10 h, followed by Baf treatment (100 nM) for 2 h before harvest and immunoblotted with LC3 and GAPDH antibodies. Increase in LC3-II levels on Baf treatment is indicative of functional autophagy flux. Numbers below the blot indicate ratio of LC3-II/GAPDH, calculated using Image J. (C) Bar graph shows relative quantitation of LC3 expression in Baf treated cells normalized to GAPDH from three independent experiments. (D-E) Cells were treated as described for panel A, and lysates were blotted for p62 and GAPDH. (E) Bar graph shows quantitation of p62 levels normalized to GAPDH from three independent experiments. (F) Relative mRNA levels of p62 in cells treated as described above. (G-H) mTOR downstream signaling was checked by measuring the proteins level of p-T386S6K1, S6K1, p-4E-BP1(Thr37/46) and 4E-BP1 antibodies. Torin1 treatment was used as a positive control. Data is representative of three independent experiments. One-way ANOVA was used to determine statistical significance, *$P < 0.05$, **$P < 0.01$, ***$P < 0.001$.

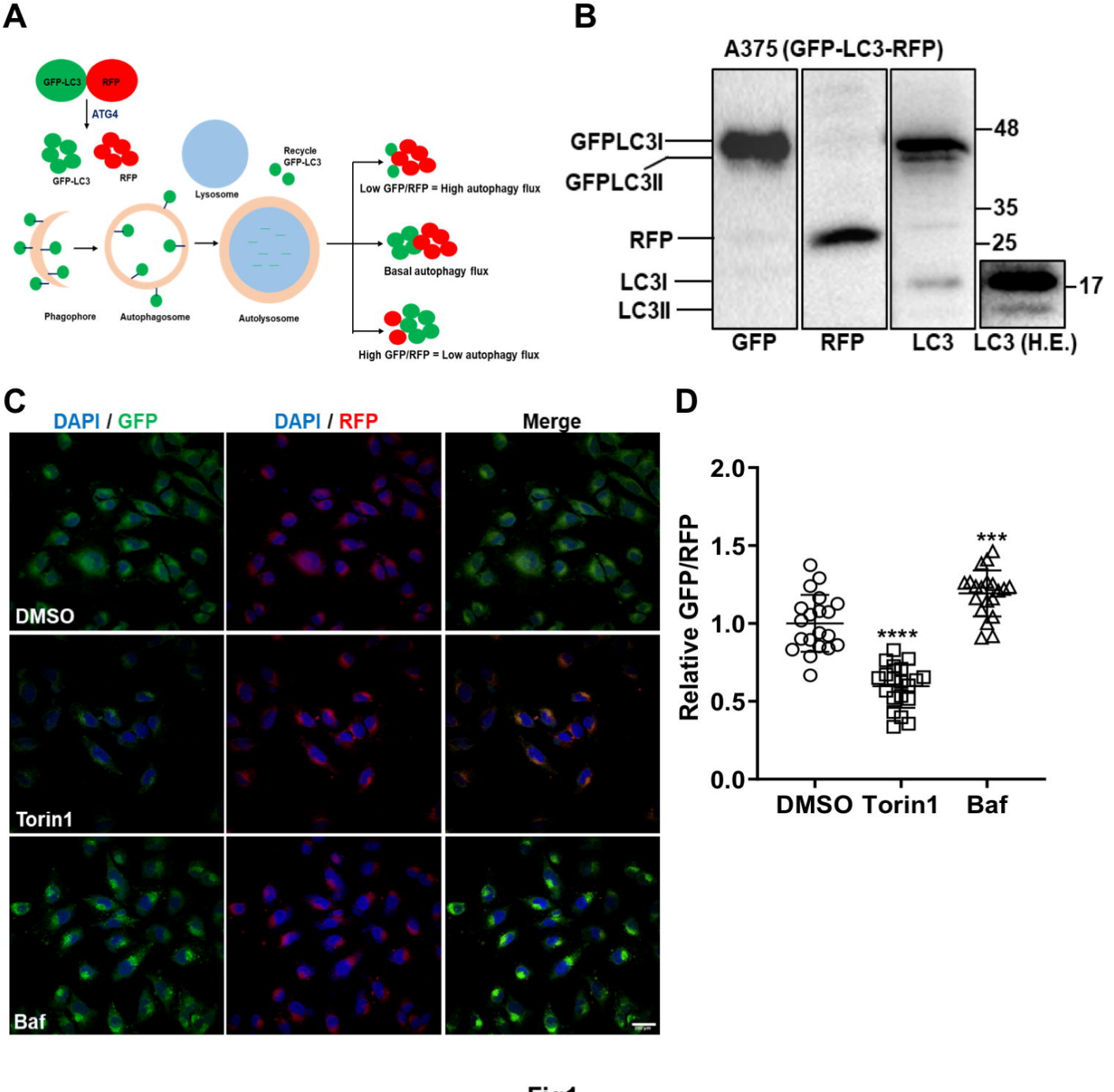
A
GFP-LC3
RFP
ATG4
GFP-LC3
RFP
Lysosome
Recycle
GFP-LC3
Low GFP/RFP = High autophagy flux
Basal autophagy flux
High GFP/RFP = Low autophagy flux
Phagophore
Autophagosome
Autolysosome
B
A375 (GFP-LC3-RFP)
GFPLC3I
GFPLC3II
RFP
LC3I
LC3II
48
35
25
17
GFP
RFP
LC3
LC3 (H.E.)
C
DAPI / GFP
DAPI / RFP
Merge
DMSO
Torin1
Baf
D
Relative GFP/RFP
2.0
1.5
1.0
0.5
0.0
****
***
DMSO
Torin1
Baf

Fig1

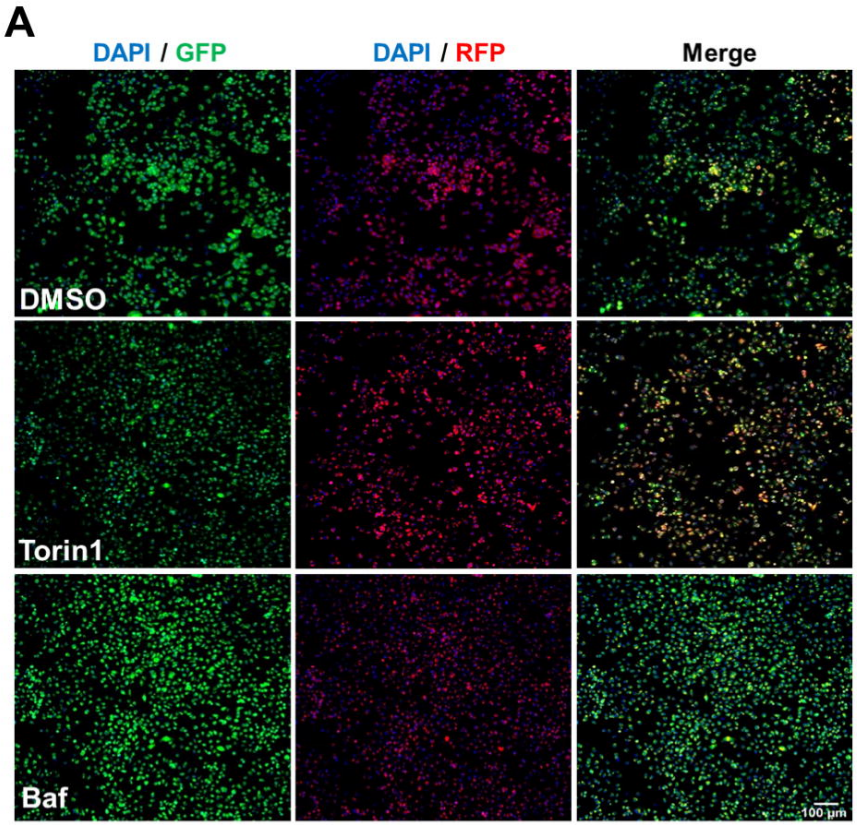
A
DAPI / GFP
DAPI / RFP
Merge
DMSO
Torin1
Baf
100 μm

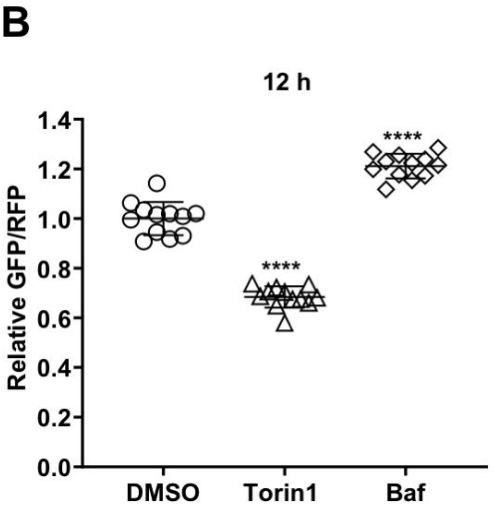
B
12 h
Relative GFP/RFP
1.4
1.2
1.0
0.8
0.6
0.4
0.2
0.0
****
****
DMSO
Torin1
Baf

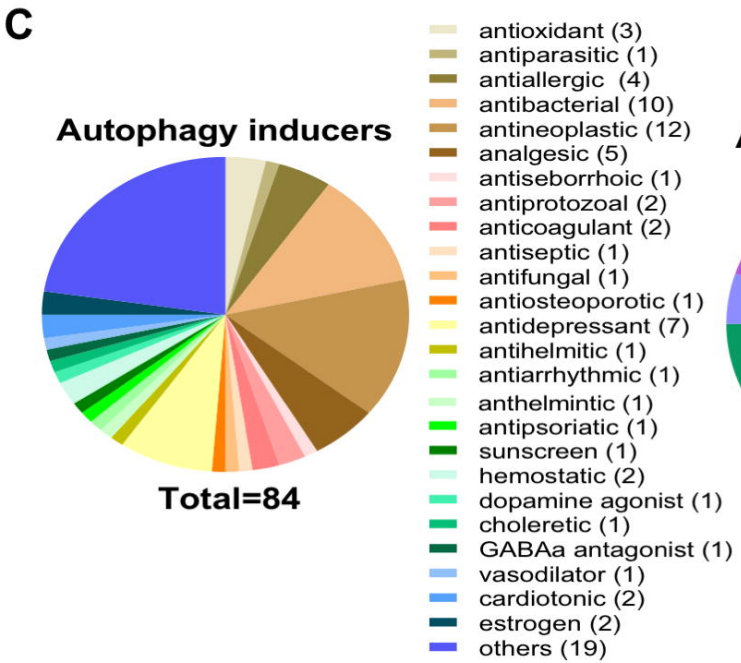
C
Autophagy inducers
Total=84
antioxidant (3)
antiparasitic (1)
antiallergic (4)
antibacterial (10)
antineoplastic (12)
analgesic (5)
antiseborrhoic (1)
antiprotozoal (2)
anticoagulant (2)
antiseptic (1)
antifungal (1)
antiosteoporotic (1)
antidepressant (7)
antihelmitic (1)
antiarrhythmic (1)
anthelmintic (1)
antipsoriatic (1)
sunscreen (1)
hemostatic (2)
dopamine agonist (1)
choleretic (1)
GABAa antagonist (1)
vasodilator (1)
cardiotonic (2)
estrogen (2)
others (19)

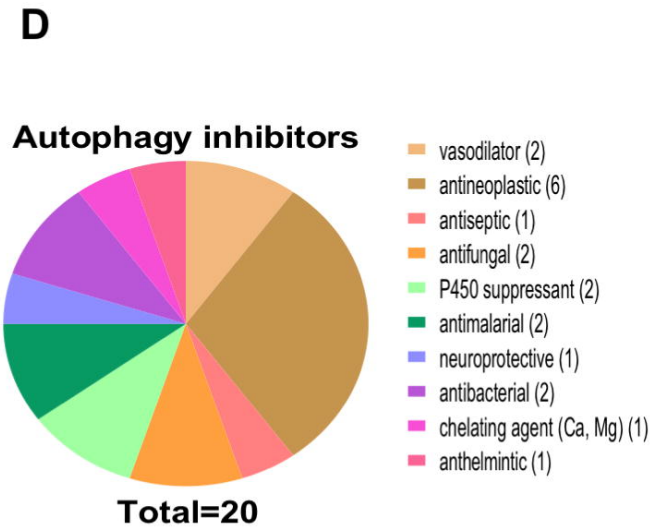
D
Autophagy inhibitors
Total=20
vasodilator (2)
antineoplastic (6)
antiseptic (1)
antifungal (2)
P450 suppressant (2)
antimalarial (2)
neuroprotective (1)
antibacterial (2)
chelating agent (Ca, Mg) (1)
anthelmintic (1)

Fig2

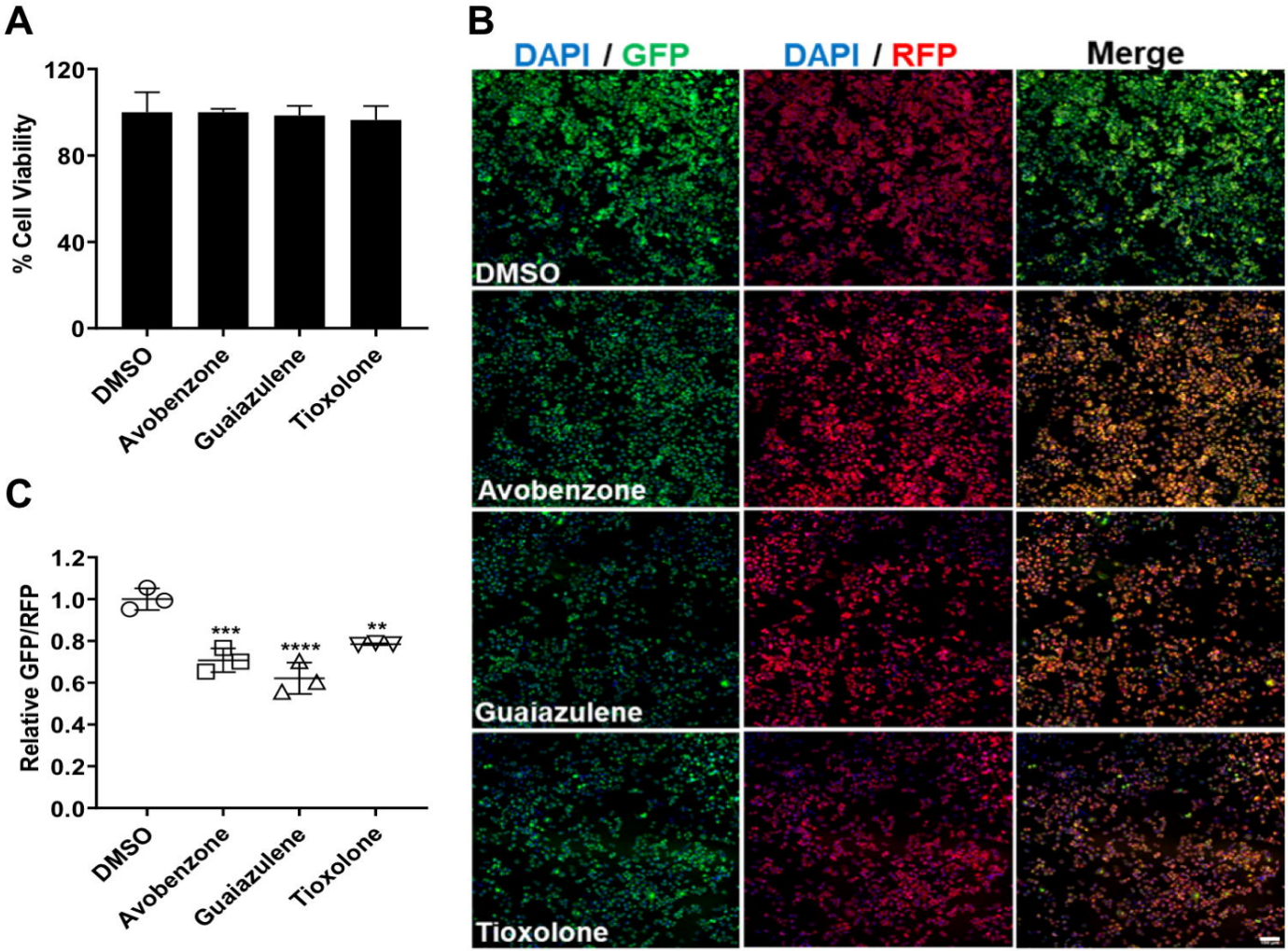
A
% Cell Viability
120
80
40
0
DMSO
Avobenzone
Guaiazulene
Tioxolone
B
DAPI / GFP
DAPI / RFP
Merge
DMSO
Avobenzone
Guaiazulene
Tioxolone
C
Relative GFP/RFP
1.2
1.0
0.8
0.6
0.4
0.2
0.0
***
****
**
DMSO
Avobenzone
Guaiazulene
Tioxolone

Fig3

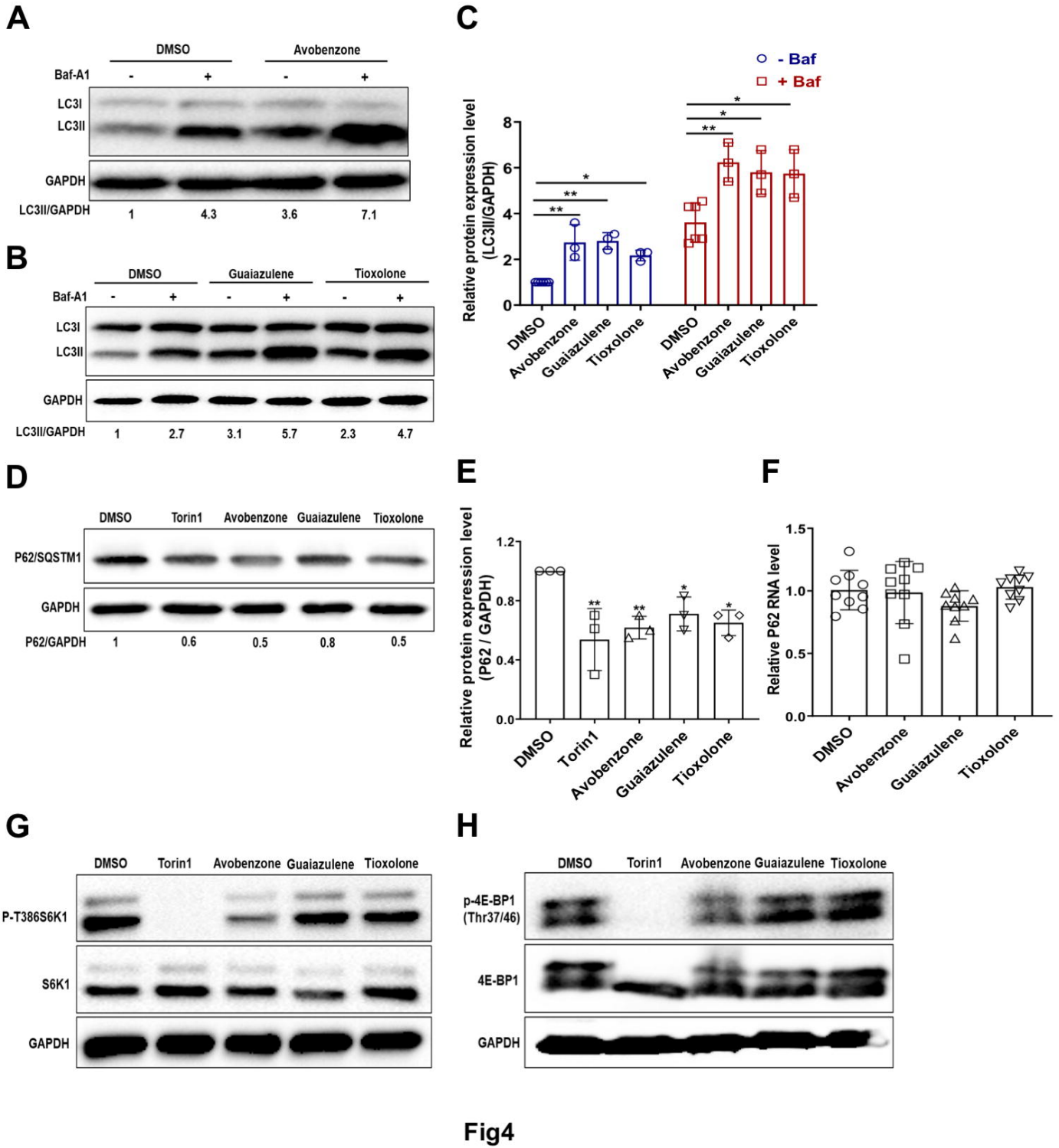
A
DMSO
Avobenzone
Baf-A1
LC3I
LC3II
GAPDH
LC3II/GAPDH
1
4.3
3.6
7.1
B
DMSO
Guaiazulene
Tioxolone
Baf-A1
LC3I
LC3II
GAPDH
LC3II/GAPDH
1
2.7
3.1
5.7
2.3
4.7
C
- Baf
+ Baf
Relative protein expression level (LC3II/GAPDH)
DMSO
Avobenzone
Guaiazulene
Tioxolone
D
DMSO
Torin1
Avobenzone
Guaiazulene
Tioxolone
P62/SQSTM1
GAPDH
P62/GAPDH
1
0.6
0.5
0.8
0.5
E
Relative protein expression level (P62 / GAPDH)
F
Relative P62 RNA level
G
P-T386S6K1
S6K1
GAPDH
H
p-4E-BP1 (Thr37/46)
4E-BP1
GAPDH

Fig4